New Journal of Physics
The open access journal at the forefront of physics

Deutsche Physikalische Gesellschaft DPG IOP Institute of Physics

Valley–spin Seebeck effect in heavy group-IV monolayers

New Journal of Physics
The open access journal at the forefront of physics

Deutsche Physikalische Gesellschaft DPG
IOP Institute of Physics

Published in partnership with: Deutsche Physikalische Gesellschaft and the Institute of Physics

OPEN ACCESS

RECEIVED
29 November 2016

REVISED
4 March 2017

ACCEPTED FOR PUBLICATION
13 April 2017

PUBLISHED
5 June 2017

PAPER

Valley–spin Seebeck effect in heavy group-IV monolayers

Xuechao Zhai[1], **Shengdong Wang**[2] **and Yan Zhang**[2]

[1] Information Physics Research Center, College of Science, Nanjing University of Posts and Telecommunications, Nanjing, 210023, People's Republic of China
[2] College of Electronic Science and Engineering, Nanjing University of Posts and Telecommunications, Nanjing, 210023, People's Republic of China

E-mail: zxc@njupt.edu.cn

Keywords: spintronics, valleytronics, Seebeck effect, group-IV monolayers

Abstract

Akin to electron spin, the valley has become another highly valued degree of freedom in modern electronics, specifically after tremendous studies on monolayers of group-IV materials, i.e. graphene, silicene, germanene and stanene. Except for graphene, the other heavy group-IV monolayers have observable intrinsic spin–orbit interactions due to their buckled structures. Distinct from the usual electric or optical control of valley and spin, we here employ a temperature difference to drive electron motion in ferromagnetic heavy group-IV monolayers via designing a caloritronic device locally modulated by an interlayer electric (E_z) field. A unique valley–spin Seebeck (VSS) effect is discovered, with the current contributed only by one (the other) valley and one (the other) spin moving along one (the opposite) direction. This effect is suggested to be detected below the critical temperature about 18 K for silicene, 200 K for germanene and 400 K for stanene, arising from the characteristic valley–spin nondegenerate band structures tuned by the E_z field, but cannot be driven in graphene without spin–orbit interaction. Above the critical temperature, the VSS effect is broken by overlarge temperature broadening. Besides the temperature, it is also found that the E_z field can drive a transition between the VSS effect and the normal spin Seebeck effect. Further calculations indicate that the VSS effect is robust against many realistic perturbations. Our research represents a conceptually but substantially major step towards the study of the Seebeck effect. These findings provide a platform for encoding information simultaneously by the valley and spin quantum numbers of electrons in future thermal-logic circuits and energy-saving devices.

1. Introduction

The study of Dirac electrons, as inspired by the rise of graphene since its fabrication in 2004, has made fruitful achievements in the most recent decade [1–5]. Particularly, two-dimensional (2D) heavy group-IV materials as graphene-like materials, including silicene, germanene and stanene, have attracted considerable research in the last five years owing to their controllable Dirac nature [6–14]. Distinct from graphene, electrons in the other 2D heavy group-IV monolayers have an observable intrinsic spin–orbit interaction because of their buckled structures [9–11, 15]. Significantly, the low-energy Dirac electrons in these materials can feel multiple degrees of freedom, involving charge, spin, valley and sublattice-pseudospin. Here, the 'valley' benefits from the fact that the Dirac electrons locate around two inequivalent points in the first Brillouin region. Up to now, many spin–valley related phenomena have been explored theoretically in heavy group-IV monolayers, such as the high-temperature quantum spin Hall effect [6], valley-polarized quantum anomalous Hall effect [11], topological superconducting effect [13], spin–valley filtering effect [16–18] and bipolar spin–valley diode effect [19]. Any of these predictions, if verified in experiment, can provide giant opportunities not only for the development of physics and material science but also for future technology applications.

To control the valley and spin in 2D Dirac materials, people usually adopt electric and optical methods to obtain valley-polarized or spin-polarized detectable effects [20–28], whereas only limited work has utilized the

temperature difference to understand the valley Seebeck effect [29, 30] or spin Seebeck effect [31–34], which can explore the possibility of directly converting heat into electrical power. Phenomenologically, the valley (spin) Seebeck effect indicates currents from two different valleys (spins) flowing in opposite directions. Experimentally, based on the magnon-driven or phonon-dragged mechanisms [35–38], great progress has recently been made in detecting the spin Seebeck effect, in magnetic materials NiFe [39], GaMnAs [40], $LaY_3Fe_5O_{12}$ [41] and MnF_2 [42] as well as non-magnetic metal InSb [43]. With attention to the recent valley–spin related experiments in graphene [44–47], there is reason to believe that the valley Seebeck effect or spin Seebeck effect should also be observed in 2D heavy group-IV materials.

In spite of many previous findings related to spin and valley, we notice that no one has ever proved whether the spin Seebeck effect and valley Seebeck effect could coexist in a real condensed-matter system. By studying the temperature-driven valley–spin transport in a designed ferromagnetic device locally modulated by an interlayer electric (E_z) field, we here discover a unique phenomenon we call the valley–spin Seebeck (VSS) effect, for which the current is contributed only by one (the other) valley and one (the other) spin moving along one (the opposite) direction. This effect surely reflects the coexistence of the spin Seebeck effect and valley Seebeck effect, and is suggested to be detected below the critical temperature 18 K for silicene, 200 K for germanene and 400 K for stanene, attributed to the specific valley–spin nondegenerate band structures, but cannot be driven in graphene without spin–orbit interaction. Above the critical temperature, the VSS effect disappears because of overlarge source-temperature broadening, independent of temperature difference. Besides the temperature, the VSS effect can also be turned on and off by the E_z field. It is further demonstrated that the VSS effect is robust against many realistic perturbations. Our findings pave the way for 2D heavy group-IV materials applied in future thermal-logic circuits and energy-saving devices.

2. Design principle for the valley–spin Seebeck effect

For any temperature-driven caloritronic device, two heat reservoirs are requisite: one is a high-temperature source (S), the other is a low-temperature drain (D). We here use $T_{S(D)}$ to describe the temperature of S (D). We define the direction of the current from S to D as positive. Because electrons in heavy group-IV monolayers have valley and spin degrees of freedom, the current should be valley–spin dependent. Below we use η (s) to denote the valley (spin) index. According to the generalized Laudauer–Büttiker approach [18, 29–32], the current driven by temperature difference $T_{SD} = T_S - T_D$ can be expressed as

$$I_\eta^s(T_S, T_D) = \frac{e}{h}\int_{-\infty}^{+\infty} d\varepsilon\, \mathcal{T}_\eta^s(\varepsilon)[f_S(\varepsilon, T_S) - f_D(\varepsilon, T_D)], \quad (1)$$

where $e = -1.6 \times 10^{-19}$ C is the electron charge, h is Planck's constant, $f_{S(D)}$ denotes the Fermi–Dirac distribution function and satisfies $f_{S(D)}(\varepsilon, T_{S(D)}) = 1/[\exp(\varepsilon - \varepsilon_F)/k_B T_{S(D)} + 1]$. $\mathcal{T}_\eta^s$ represents the number of valley–spin dependent transmission modes, depending on the detailed device structure. Because silicene, germanene and stanene are semiconductors with small spin–orbit band gaps less than 0.2 eV, the temperature primarily plays the role of exciting thermoelectrons here [31–33], different from that of exciting magnons in ferromagnetic insulators [41]. From the distribution difference $f_S - f_D$ in equation (1), we judge that electrons with energy higher than the Fermi energy ε_F flow from S to D on account of $f_S - f_D > 0$, resulting in electron current $(I_e)_\eta^s < 0$. Conversely, electrons with energy lower than ε_F flow from D to S as a result of $f_S - f_D < 0$, leading to hole current $(I_h)_\eta^s > 0$. A specific case is that, if $\mathcal{T}_\eta^s$ is symmetric about the Fermi energy, the electron current and the hole current will cancel out each other, leading to no net current, i.e. $I_\eta^s = (I_e)_\eta^s + (I_h)_\eta^s = 0$. This happens in undoped pristine graphene and its derivatives with electron–hole symmetry.

To create electron–hole asymmetry near the Fermi energy it is a necessary condition to generate nonzero current, but needs to far from enough to effectively drive the VSS effect in heavy group-IV monolayers. Based on band theory, we conclude that the detailed form of $\mathcal{T}_\eta^s$ in equation (1) depends on the band-to-band tunneling mechanism, and dictates whether the valley or spin Seebeck effect happens. On the one hand, to drive the normal spin Seebeck (NSS) effect, the transmission should be electron-dominated for one spin but hole-dominated for the other spin. This requires that the band structure near the Fermi energy must be nondegenerate for two spins besides electron–hole asymmetry. This is relatively easy to realize in the ferromagnetic state of semiconductors [10, 19, 31]. On the other hand, to generate the valley Seebeck effect, one must ensure that the transmission near the Fermi energy is electron-dominated for one valley but hole-dominated for the other valley [29, 30]. This condition cannot be satisfied in a sample of silicene, germanene or stanene only in the presence of the E_z field, although the band structure is both valley-polarized and spin-polarized [10]. Conceivably, to realize the VSS effect, the transmission should be electron-dominated for one spin in one valley but hole-dominated for the other spin in the other valley. In this case, there might exist a particular energy region, inside which one valley is insulating for two spins but the other valley is conductive for only one spin. Luckily, we notice that, for heavy group-IV monolayers, the coexistence of ferromagnetic field

and E_z field could satisfy this criterion [29]. Additionally, to observe the VSS effect, the energy broadening induced by the source temperature cannot exceed the particular insulating region for two spins, or otherwise the deep-energy bands outside the band gap can break the transport feature of the VSS effect.

Here, we need to make clear how to obtain the transmission modes $\mathcal{T}_\eta^s$ in equation (1). For simplicity, the reduced Planck constant $\hbar$ is set as 1, and the Fermi velocity υ_F ($5.5 \times 10^5\,\mathrm{m\,s^{-1}}$ for silicene, $4.6 \times 10^5\,\mathrm{m\,s^{-1}}$ for germanene, $4.9 \times 10^5\,\mathrm{m\,s^{-1}}$ for stanene [10, 15]) is set as 1. For a sample of width W, the total transmission modes are generally obtained by [19, 29]

$$\mathcal{T}_\eta^s(\varepsilon) = N_0 \frac{k}{\lambda} \int_0^{\pi/2} \mathrm{d}\phi\ T_\eta^s(\varepsilon,\ \phi)\cos\phi, \tag{2}$$

where k, ϕ are the modulus and angle of the wave-vector, $N_0 = (2W/\pi)\,\lambda$ represents the reduced constant with the dimension of density of states, and $T_\eta^s(\varepsilon,\ \phi)$ describes the angle-dependent transmission for each mode. Then the spin–valley dependent current is calculated from equation (1) as

$$I_\eta^s = -I_0 \int_{-\infty}^{+\infty} \mathrm{d}\varepsilon \frac{k}{\lambda}(f_S - f_D) \int_0^{\pi/2} \mathrm{d}\phi T_\eta^s(\varepsilon,\ \phi)\cos\phi. \tag{3}$$

where the constant $I_0 = -N_0 e/h > 0$ is used as the reduced value of I_η^s.

3. Realization of the valley–spin Seebeck effect

At the top of figure 1(a), we show our proposed caloritronic field effect transistor device, including S, D and G (the central gate region controlled by an E_z field). A ferromagnetic field with strength M is uniformly applied in the whole sample. From previous first-principles calculations, it is known that the low-energy electrons in heavy group-IV monolayers can be described by an effective Hamiltonian which reads $H_0 = (\eta\tau_x k_x + \tau_y k_y) + \eta\lambda\tau_z\sigma_z$ [20–23], where λ (3.9 meV for silicene, 43 meV for germanene, 100 meV for stanene) represents the spin–orbit coupling, $\eta = +(-)$ labels valley K (K'), and τ_i, σ_i ($i = x,\ y,\ z$) describe the Pauli matrices of sublattice pseudospin and electron real-spin respectively. Although Rashba-type spin–orbit couplings as perturbations in these heavy group-IV monolayers exist in principle, they play little role even under external fields in studying the band structures and transport properties [6, 10]. Thus the low-energy effective Hamiltonian here can be expressed as

$$H = H_0 + M\sigma_z - \ell E_z \tau_z Q(x), \tag{4}$$

where the second term indicates the ferromagnetic field, the third term represents the E_z field with $Q(x) = \Theta(x) - \Theta(x - L)$. Herein, $\Theta(x)$ is the Heaviside function, and ℓ denotes the interlayer distance. After matrix diagonalization, the energy bands are solved as

$$\varepsilon(k) = sM + \alpha\sqrt{k^2 + [\ell E_z Q(x) - s\eta\lambda]^2}\,, \tag{5}$$

The energies at valleys K, K' ($k = 0$) read $\epsilon_\alpha^{s,\eta} = sM + \alpha|\ell E_z Q(x) - s\eta\lambda|$. In regions S and D, it is found that the transport-forbidden regions for spin-up and spin-down electronic states read, respectively, $(-\lambda + M,\ \lambda + M)$ and $(-\lambda - M,\ \lambda - M)$, identical for two different valleys. In region G, the valley degeneracy is destroyed by locally applying ℓE_z, and the band gap regions for spin-up and spin-down bands are obtained, respectively, as $(\lambda_F - |\ell E_z - \eta\lambda|,\ \lambda_F + |\ell E_z - \eta\lambda|)$ and $(-\lambda_F - |\ell E_z + \eta\lambda|,\ -\lambda_F + |\ell E_z + \eta\lambda|)$. The mutual insulating region for two spins is $(\lambda_F - |\ell E_z - \eta\lambda|,\ -\lambda_F + |\ell E_z + \eta\lambda|)$ if it exists. The energy bands for S, D and G, at $\ell E_z = 2\lambda$ and $\varepsilon_F = 0$, are shown at the bottom of figure 1(a). There are two factors that lead to the forbidden transmission: (i) spin–valley dependent band gaps provided by S, D and G, (ii) spin mismatch between S, D and G. The shaded regions $(-2\lambda,\ 0) \cup (0,\ 2\lambda)$ are just the mutual insulating regions for two spins to drive the VSS effect, and the bands in region G are electron-dominated for one spin in one valley but hole-dominated for the other spin in the other valley.

To obtain information on I_η^s, it is still needed to solve T_η^s in equation (3). Based on quantum mechanics, we derive the transmission amplitude by matching the wave functions at the interfaces $x = 0,\ L$ as

$$t_\eta^s(\phi) = \frac{2\beta\beta' \mathrm{e}^{\mathrm{i}\kappa L}\cos\phi\,[\sin(q_x L)\mathrm{e}^{-\mathrm{i}\eta\theta} + \mathrm{i}\cos\theta']}{F\,[\beta\sin(q_x L)\mathrm{e}^{-\mathrm{i}\eta\phi} + \mathrm{i}\beta'\cos\theta'] + \mathrm{i}F'\beta'\cos\theta}, \tag{6}$$

where $\beta = (\varepsilon + s\eta\lambda - sM)/k$, $\beta' = (\varepsilon + s\eta\lambda - sM - \ell E_z)/q$, $\kappa = q\cos\theta - k\cos\phi$, $\theta = \pi - \arcsin(k\sin\phi/q)$. The wave-vector modulus in regions S, D and G are obtained respectively as $k = \sqrt{(\varepsilon - sM)^2 - \lambda^2}$, $q = \sqrt{(\varepsilon - sM)^2 - (\ell E_z - s\eta\lambda)^2}$. The angular dependent functions F, F' are obtained as $F = \beta\mathrm{e}^{\mathrm{i}\eta\phi} + \beta'\mathrm{e}^{-\mathrm{i}\eta\theta}$, $F' = \beta\mathrm{e}^{-\mathrm{i}\phi'} - \beta'\mathrm{e}^{-\mathrm{i}\theta'}$, where $\phi' = \eta\phi - qL\cos\theta$ and $\theta' = \eta\theta - qL\cos\theta$. The transmission coefficient in equation (1) is then given by

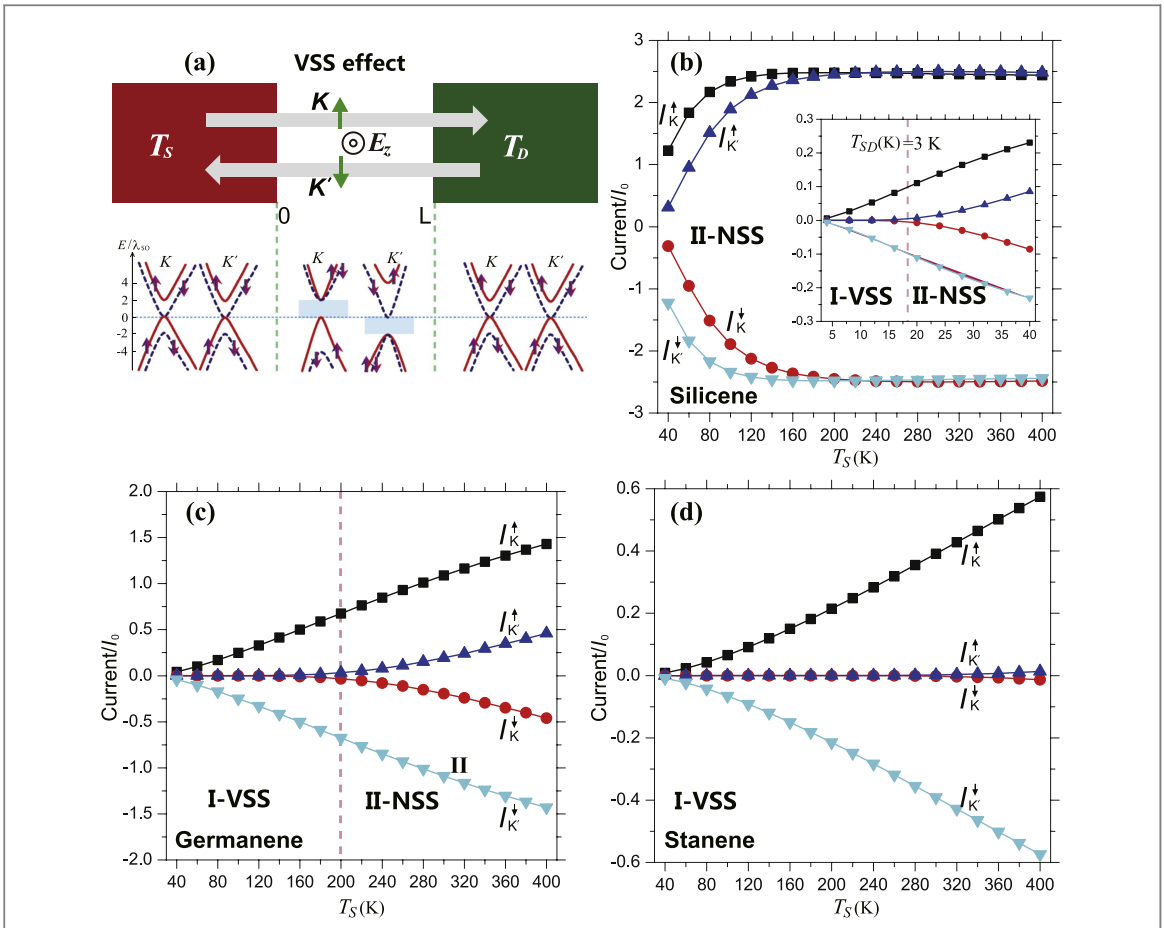

Figure 1. (a) Top: overhead view of our proposed caloritronic FET device, where the valley–spin Seebeck (VSS) effect is illustrated. The device is constructed from the left source (S) with higher temperature T_S, the right drain (D) with lower temperature T_D, and the central gate region (G) where the E_z field can be tuned by dual gates. Bottom: band-matching mechanism for the VSS effect at $\ell E_z = 2\lambda$. The shaded regions indicate the mutual transport gaps for two spins. (b)–(d) Current T_η^s versus T_S for silicene, germanene and stanene, respectively, at $\ell E_z = 2\lambda$. Two different phases are denoted, including phase I-VSS and phase II-NSS (normal spin Seebeck effect). The temperature difference is fixed at $T_{SD} = 20$ K, except for the inset in figure (b) where $T_{SD} = 3$ K.

$$T_\eta^s(\varepsilon, \phi) = |t_\eta^s(\phi)|^2. \tag{7}$$

Note that, for uniformity, the parameters $M = \lambda$ and $L = 50$ nm are used below to carry out the calculations and plot figures without special instructions.

In figures 1(b)–(d), we plot the current I_η^s versus the source temperature T_S for silicene, germanene and stanene, respectively, at $\ell E_z = 2\lambda$. The temperature difference is fixed at $T_{SD} = 20$ K, except for the inset in figure 1(b) where $T_{SD} = 3$ K. Two different phases are found, one is marked as I-VSS and the other is marked as II-NSS. It can be seen that the VSS effect can be observed below the critical temperature 18 K for silicene, 200 K for germanene and 400 K for stanene. The increasing critical temperature from silicene to stanene is consistent with the increasing spin–orbit interaction. The critical temperature T_c could be approximately determined by $5k_B T_c = 2M = 2\lambda$, where k_B is the Boltzmann constant. Above the critical temperature, the NSS effect is detectable. As is known, the index-change relationship of the Fermi–Dirac distribution function determines that only electronic states near the Fermi energy could contribute to the current. Consequently, the thermodynamical transition from VSS phase to NSS phase is attributed to the fact that, only if the energy broadening $5k_B T_S$ induced by the source temperature does not exceed the gap size 2λ, high-energy subbands cannot break the transport feature of the VSS effect. For the phase I-VSS, it is seen that only spin-up (down) states from valley K (K') contribute to the positive (negative) current, in agreement with the band structures in figure 1(a), where hole (electron) states contribute most to $I_K^\uparrow$ ($I_{K'}^\downarrow$). As T_S increases, the hole-dominated current $I_{K'}^\uparrow$ and the electron-dominated current $I_K^\downarrow$ become nonzero due to enhanced temperature broadening. As T_S becomes much larger than 400 K, all the values of $|I_\eta^s|$ in figures 1(c) and (d) tend to stabilize due to convergence of the integral in equation (3), just as calculated in figure 1(b).

In figure 2, we plot the curves of the current I_η^s versus the temperature difference T_{SD} for silicene (left), germanene (middle) and stanene (right), respectively, at $\ell E_z = 2\lambda$. The source temperature is fixed at $T_S = 340$ K, except for the inset in silicene where $T_S = 15$ K. It is easy to understand that, under the condition of $T_{SD} \to 0$,

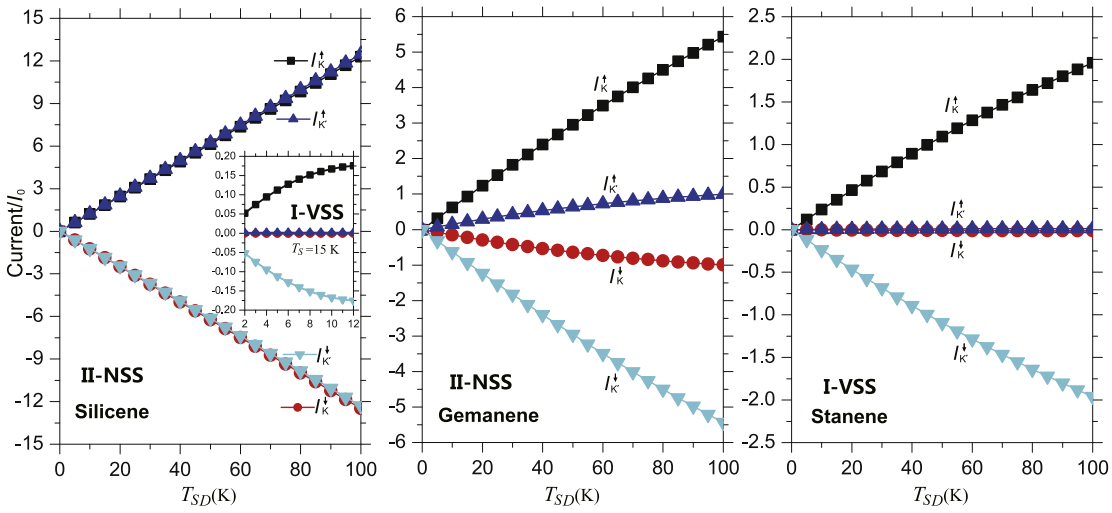

Figure 2. Reduced current I^s_η/I_0 versus temperature difference T_{SD} for silicene (left), germanene (middle) and stanene (right). The parameters are fixed at $T_S = 340$ K, $\ell E_z = 2\lambda$, while T_S is fixed at 15 K in the left-panel inset.

the driving force tends to zero and thus all the currents I^s_η tend to zero. Owing to $T_S \gg T_{SD}$, except for the inset in figure 2(a), the nonzero I^s_η curves basically increase linearly as T_{SD} increases. Also, such linear relationships can be judged from equation (3), where I^s_η under $T_{LR} \ll T_S \simeq T_D$ could be expressed as

$$I^s_\eta \simeq I_0 \frac{T_{LR}}{T_S} \int \frac{\varepsilon}{kN_0} \mathcal{T}^s_\eta(\varepsilon) \sqrt{(\varepsilon - sM)^2 - \lambda^2}\, \mathrm{d}\left(\frac{1}{e^{\varepsilon/(k_B T_S)} + 1}\right). \tag{8}$$

In the low-T_S case, the linear relationships disappear although the curves $I^s_\eta(T_{SD})$ vary monotonically, as seen from the inset in figure 2(a). In comparison with figures 1(b)–(d), T_S and ℓE_z here do not change, and hence we have reason to conclude that the presence of the VSS effect is basically independent of T_{SD}, because no new phase is induced by increasing T_{SD}. For germanene, the VSS effect could also be detected if T_S is fixed at a small value less than the critical temperature 200 K, just as shown by the inset in figure 2(a).

In figure 3, we further show the reduced current I^s_η/I_0 as a function of the electric field ℓE_z for silicene (top), germanene (middle) and stanene (bottom). The temperature conditions read $T_S = 340$ K, $T_{SD} = 40$ K, except for the left-panel inset where $T_S = 15$ K, $T_{SD} = 5$ K. The main result here is that the VSS and NSS effects could be switched to each other by tuning the E_z field. To understand this phenomenon, we need to analyze the variation of band structures in region G induced by the E_z field. As ℓE_z varies, the mutual insulating region for two spins $(\lambda_F - |\ell E_z - \eta\lambda|, -\lambda_F + |\ell E_z + \eta\lambda|)$ changes. The energy scale of this region is $\Delta E = |\ell E_z + \eta\lambda| + |\ell E_z - \eta\lambda| - 2\lambda_F$. We find the VSS effect can happen only when $\Delta E > 5k_B T_S$ is approximately satisfied. It can be checked that the critical $|\ell E_z|$-values, determined by $\Delta E = 5k_B T_S$, are approximately $3.5\lambda \simeq 5k_B T_S \simeq 150$ meV for germanene and $1.5\lambda \simeq 5k_B T_S = 150$ meV for stanene at $T_S = 340$ K, and $1.5\lambda \simeq 5k_B T_S \simeq 6$ meV for silienece at $T_S = 15$ K. If the E_z field becomes large enough, all the currents of I^s_η are turned 'off' because no electronic states near the Fermi energy can be excited due to the large band gap. Thus, to realize the VSS effect, ℓE_z should be neither too small nor too large. All these analyses agree well with the numerical curves, where the VSS effect is valid under $3\lambda < |\ell E_z| < 4.5\lambda$ for germanene and $1.5\lambda < |\ell E_z| < 3\lambda$ for stanene at $T_S = 340$ K, but $1.5\lambda < |\ell E_z| < 2.5\lambda$ for silicene at $T_S = 15$ K. In addition, the symmetry of the system decides the relation $I^s_\eta(\ell E_z) = I^s_{-\eta}(-\ell E_z)$. Physically, by changing the sign of ℓE_z (inverse electric field), the band structures between valley K and K' can be exchanged. Specifically at $\ell E_z = 0$, I^s_η and $I^s_{-\eta}$ cross due to the valley degeneracy.

Now one may wonder whether inelastic scattering at higher temperatures affects our ballistic results in figures 1–3. It is true that electron–phonon interactions should be enhanced as temperature increases due to more excited phonon modes, and thus electron mobility naturally decreases. For electron–phonon scattering, we divide it into two types: intravalley scattering and intervalley scattering. For intravalley scattering, increasing temperature cannot drive the jump between different states labeled by different valley–spin indexes due to the absence of the spin–valley flipping mechanism, but only reduces the magnitude of I^s_η. This indicates that the qualitative conclusions in the ballistic regime remain the same. For intervalley scattering, recent first-principles calculations have demonstrated that only electrons with energy more than several tens of meV or larger in silicene and germanene could feel this scattering induced by the stronger electron–phonon coupling [48], even

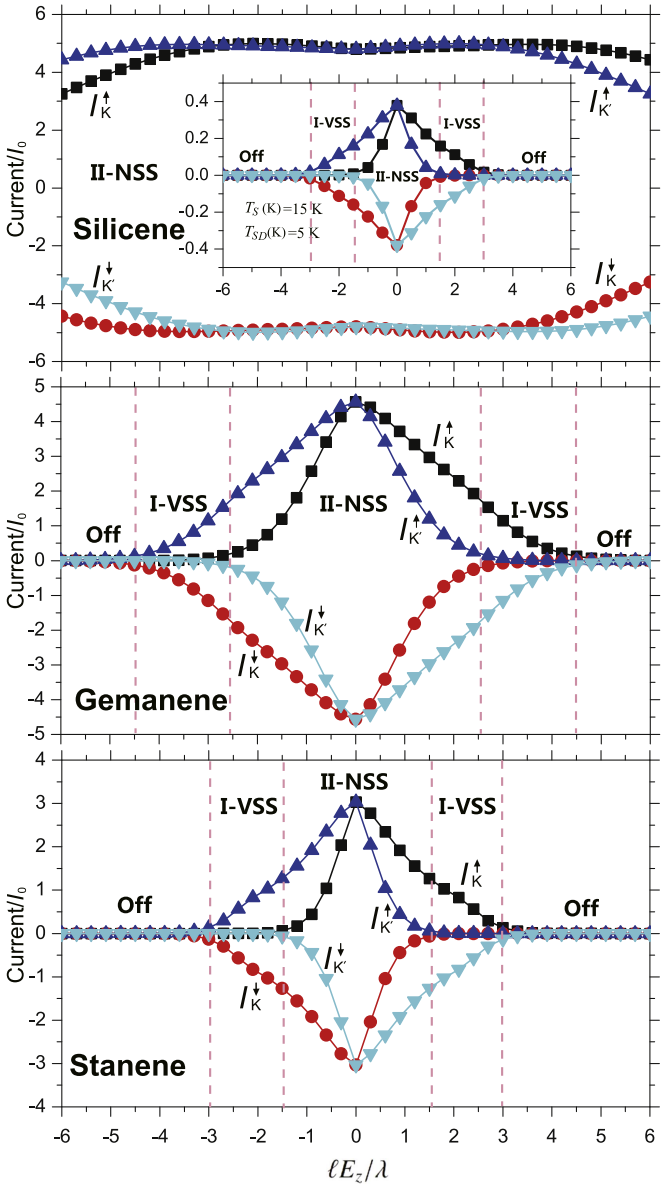

Figure 3. Reduced current I^s_η/I_0 versus the electric-field parameter ℓE_z for silicene (top), germanene (middle) and stanene (bottom). The parameters are chosen at $T_S = 340$ K, $T_{SD} = 40$ K except for the silicene inset, where $T_S = 15$ K, $T_{SD} = 5$ K.

near room temperature. Consequently, it is reasonable to believe that inelastic scattering has little effect on the detectable properties of the VSS effect in our considered range of temperatures.

Additionally, note that the net current contributed by spin-up and spin-down electrons always flows in opposite directions (pure spin current) in figures 1–3 and indeed the spin polarizability is 100%, benefiting from the completely spin-polarized subbands near the Fermi energy (see figure 1(a)). Thus it is not necessary to define the degree of spin polarization here. Nevertheless, one can notice that the NSS in figure 2(b) for gemanene is different from that in figure 2(a) for silicene, resulting from different degrees of valley polarization ρ_v. Further considering that the total current contributed by two opposite directions is always zero in figures 1–3 due to symmetry, it is difficult to define an overall effective ρ_v for bidirectional transport, but one can still treat ρ_v separately for positive and negative currents via a definition $\rho_v = \sum_s (I^s_K - I^s_{K'})/\sum_{\eta,s} I^s_\eta$, where all the possible currents I^s_η are either nonnegative (positive transport) or nonpositive (negative transport). For II-NSS in figure 2(a), $\rho_v \simeq 0$ for both positive and negative currents, while $|\rho_v| \simeq 70\%$ for II-NSS in figure 2(b). Distinct from II-NSS, it must satisfy $|\rho_v| \simeq 100\%$ in both directions for I-VSS. To distinguish the boundary between I-VSS and II-NSS in figures 1–3 more strictly, we here use a relatively accurate approximation that if the current component I^s_η is less than 5% of the total current, one can ignore this component.

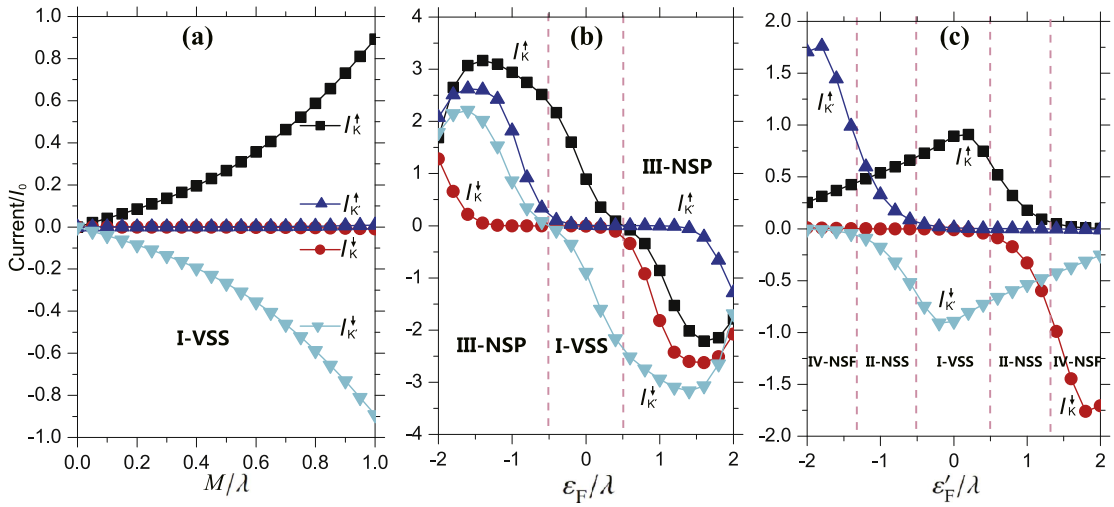

Figure 4. Robustness of the VSS effect in realistic conditions for stanene at $T_S = 340$ K, $T_{SD} = 40$ K, $\ell E_z = 2\lambda$. (a) Reduced current I^s_η/I_0 versus the ferromagnetic field M. (b) Reduced current I^s_η/I_0 versus the Fermi energy E_F, which is uniform for the whole silicene sample. NSP denotes the normal spin polarized phase III. (c) Reduced current I^s_η/I_0 versus the Fermi energy E'_F in region G while the Fermi energy in regions S and D reads $E_F = 0$. NSF denotes the normal spin filtering phase IV.

4. Robustness of the valley–spin Seebeck effect

Since we have obtained information for how to realize the VSS effect in silicene, germanene and stanene, it is still necessary to discuss the robustness of the VSS effect in some real complex experimental conditions. Below, we take stanene for instance and study the influence of the ferromagnetic field and the Fermi energy on the VSS effect near room temperature. The fixed parameters read $T_S = 340$ K, $T_{SD} = 40$ K, $\ell E_z = 2\lambda$. Note that the conclusions for stanene here are universally valid for germanene and silicene under lower T_S.

Firstly, we show the influence of ferromagnetic field M on the VSS effect in figure 4(a). Our results indicate that the VSS effect is always robust at $M \leqslant \lambda$. This result depends on such a fact that the ferromagnetic field does not essentially change the electron–hole asymmetry in figure 1(a) in spite of band variations. Further considering that the ferromagnetic field has been successfully introduced in graphene by the proximity effect of the ferromagnetic insulating substrate [49], it is reasonable to believe that the ferromagnetic field could also be applied in silicene, germanene and stanene. In this sense, one can easily observe the VSS effect in a large range of M-strength. In addition, provably, the length L of region G does also not change the realization of the VSS effect.

Secondly, we consider a stanene sample that is uniformly doped ($\varepsilon_F \neq 0$) for both S, D and G. It is verified that the VSS effect is robust under $|\varepsilon_F| < 0.5\lambda$, beyond which phase III-NSP (normal spin polarized current) with weak spin–valley polarizaton works. Due to the specific valley–spin symmetry for the band structures in figure 1(a), $I^s_\eta(\varepsilon_F) = -I^{-s}_{-\eta}(-\varepsilon_F)$ is always valid here. This means we only need to analyze the curves when ε_F has positive values. By changing ε_F, the band structures remain the same while the electron–hole asymmetry varies. The magnitude of I^s_η is determined by the degree of asymmetry: the stronger the electron–hole asymmetry, the larger the current is. As ε_F increases from 0 to 2λ, the current $I^\uparrow_K$ first decreases to zero then changes its sign because the electron–hole asymmetry about ε_F first decreases (hole-dominated, $I^\uparrow_K > 0$) then increases (electron-dominated, $I^\uparrow_K < 0$), as expected from figure 1(a); $I^\downarrow_K$ can also be turned on as the temperature broadening exceeds the corresponding valley–spin conduction band (electron-dominated, $I^\downarrow_K < 0$); $I^\uparrow_{K'}$ (electron-dominated, $I^\uparrow_{K'} < 0$) is turned on when the temperature broadening is larger than the corresponding transport gap; the current $I^\downarrow_{K'}$ is always electron-dominated (see figure 1(a)), and thus $I^\downarrow_{K'} < 0$. As a result, the NSP phase happens as ε_F increases.

Thirdly, we further consider the robustness of the VSS effect on the Fermi energy ε'_F in region G for a sample that is undoped ($\varepsilon_F = 0$) in regions S and D in figure 4(c). It is found that the VSS effect is robust at $|\varepsilon'_F| < 0.5\lambda$, beyond which phases II-NSS and IV-NSF (normal spin-filtering phase) can be gradually observed as $|\varepsilon'_F|$ increases. Different from bidirectional current in the Seebeck effect, the NSF phase only supports unidirectional current. Depending on the system symmetry, $I^s_\eta(\varepsilon'_F) = -I^{-s}_{-\eta}(-\varepsilon'_F)$ always holds, and thus we only need to analyze the curves when ε'_F has positive values. By changing ε'_F, the band structures in region G do not change while the electron–hole asymmetry varies, just as demonstrated in figure 4(b). As ε'_F increases from 0 to 2λ, $I^\uparrow_K$ (hole-dominated, $I^\uparrow_K > 0$) gradually tends to zero because the corresponding transport gap increases; when $\varepsilon'_F > 0.5\lambda$, $I^\downarrow_K$ (electron-dominated, $I^\downarrow_K < 0$, as seen from figure 1(a)) could be turned on; $I^\uparrow_{K'}$ is always turned

off because $5k_B T_S$ cannot overreach the corresponding transport-gap region; $I^{\downarrow}_{K'}$ (electron-dominated, $I^{\downarrow}_{K'} < 0$) decreases because the transport gap keeps away from the Fermi energy. No surprise is that the NSS phase can occur. At $1.3 < \varepsilon'_F < 2$, only spin-up states dominated by electrons from two valleys contribute to the current ($I^{\uparrow}_{\eta} < 0$, $I^{\downarrow}_{\eta} \simeq 0$), and thus the NSF effect is observed.

Lastly, we discuss the influence of some complex conditions on the VSS effect. Firstly, in terms of band changes, the Rashba interactions do not change the valley–spin dependent band gap although there is spin splitting outside the valley points [13–17]. Actually, for silicene, germanene and stanene, the spin splitting induced by Rashba perturbations plays little role in affecting the spin–valley transport, as proved by previous first-principles calculations [10]. Secondly, note that our concerned VSS effect is based on bulk states of the materials but not edge states [47] and thus could be detected in experiments more easily due to the stronger signal, although this VSS effect has some common transport features to valley-polarized quantum spin Hall edge states [28]. Thirdly, a real sample of heavy group-IV monolayers also inevitably contains atomic defects in the bulk, such as bits of vacancies [12, 49], which induce variations of supercell bands. To realize the VSS effect, the defect ratio cannot exceed 8%, otherwise the VSS effect is broken by defect states that contribute to the current [50]. Fourthly, to avoid intervalley scattering, local gates are suggested to deplete edge carriers and form gate-defined sample edges, near which the variations of edge potential do not change the delectability of the VSS effect owing to the negligible proportion of edge atoms [19]. In short, although there has been little experimental study about the temperature-driven electron motion in heavy group-IV monolayers so far, we still have sufficient reason to believe that the VSS effect discussed here is detectable by developing the latest experimental detection techniques on valley or spin in graphene [44–47]. To be sure, our results here advance our previous work about the realization of NSS or valley Seebeck effects as well as confirm the rough prediction of the coexistence of these two effects [51].

5. Conclusion

In summary, based on monolayers of heavy group-IV materials, we have designed a caloritronic device locally modulated by an interlayer electric field to realize a unique valley–spin Seebeck (VSS) effect, which supports bidirectional transport with each net current direction locked by both valley and spin. Associated with the strength of the spin–orbit band gap, such a VSS effect is suggested to be detectable using current experimental technology below the critical temperature 18 K for silicene, 200 K for germanene and 400 K for stanene, arising from the specific valley–spin band structures. We have also found that above the critical temperature, the VSS effect may be broken by overlarge temperature broadening, basically independent of temperature difference. Besides the temperature, the local electric field can also drive a transition between the VSS and normal spin Seepbeck effects by tuning the band structures. Furthermore, we have proved that the VSS effect found here is robust against many realistic perturbations. These findings provide new insights to apply two-dimensional heavy group-IV materials in future information procession (encoding information simultaneously by valley and spin) in thermal logic circuits and low-dissipation devices.

Acknowledgments

This work was supported by the National Natural Science Foundation of China (Grant No. 11504179), the Natural Science Foundation of Jiangsu Province (Grant No. BK20150830), NUPTSF (Grant No. NY214193), and the State Key Program for Basic Research of China (Grant No. 2015CB921202).

References

[1] Novoselov K S, Geim A K, Morozov S V, Jiang D, Katsnelson M I, Grigorieva I V, Dubonos S V and Firsov A A 2005 Two-dimensional gas of massless Dirac fermions in graphene *Nature* **438** 197–200
[2] Pesin D and MacDonald A H 2012 Spintronics and pseudospintronics in graphene and topological insulators *Nat. Mater.* **11** 409–16
[3] Xu M, Liang T, Shi M and Chen H 2013 Graphene-like two-dimensional materials *Chem. Rev.* **113** 3766–98
[4] Han W, Kawakami R K, Gmitra M and Fabian J 2014 Graphene spintronics *Nat. Nanotechnol.* **9** 794–807
[5] Fiori G, Bonaccorso F, Iannaccone G, Palacios T, Neumaier D, Seabaugh A, Banerjee S K and Colombo L 2014 Electronics based on two-dimensional materials *Nat. Nanotechnol.* **9** 768–79
[6] Liu C-C, Feng W and Yao Y 2011 Quantum spin Hall effect in silicene and two-dimensional germanium *Phys. Rev. Lett.* **107** 076802
[7] Vogt P, De Padova P, Quaresima C, Avila J, Frantzeskakis E, Asensio M C, Resta A, Ealet B and Le Lay G 2012 Silicene: compelling experimental evidence for graphene-like two-dimensional silicon *Phys. Rev. Lett.* **108** 155501
[8] Ni Z, Liu Q, Tang K, Zheng J, Zhou J, Qin R, Gao Z, Yu D and Lu J 2012 Tunable bandgap in silicene and germanene *Nano Lett.* **12** 113–8
[9] Ezawa M 2012 Valley-polarized metals and quantum anomalous Hall effect in silicene *Phys. Rev. Lett.* **109** 055502
[10] Tsai W-F, Huang C-Y, Chang T-R, Lin H, Jeng H-T and Bansil A 2013 Gated silicene as a tunable source of nearly 100% spin-polarized electron *Nat. Commun.* **4** 1500

[11] Pan H, Li Z, Liu C-C, Zhu G, Qiao Z and Yao Y 2014 Valley-polarized quantum anomalous Hall effect in silicene *Phys. Rev. Lett.* **112** 106802
[12] Tao L, Cinquanta E, Chiappe D, Grazianetti C, Franciulli M, Dubey M, Molle A and Akinwande D 2015 Silicene field-effect transistors operating at room temperature *Nat. Nanotechnol.* **10** 227–31
[13] Ezawa M 2015 Antiferromagnetic topological superconductor and electrically controllable Majorana fermions *Phys. Rev. Lett.* **114** 056403
[14] Zhu F-F, Chen W-J, Xu Y, Gao C-L, Guan D-D, Liu C-H, Qian D, Zhang S-C and Jia J-F 2015 Epitaxial growth of two-dimensional stanene *Nat. Mater.* **14** 1020–5
[15] Xu Y, Zhou X and Jin G 2016 Detecting topological phases in silicene by anomalous Nernst effect *Appl. Phys. Lett.* **108** 203104
[16] Soodchomshom B 2014 Perfect spin-valley filter controlled by electric field in ferromagnetic silicene *J. Appl. Phys.* **115** 023706
[17] Wang D, Huang Z, Zhang Y and Jin G 2016 Spin-valley filter and tunnel magnetoresistance in asymmetrical silicene magnetic tunnel junctions *Phys. Rev.* B **93** 195425
[18] Zhai X and Jin G 2016 Completely independent electrical control of spin and valley in a silicene field effect transistor *J. Phys.: Condens. Matter* **28** 355002
[19] Zhai X, Zhang S, Zhao Y, Zhang X and Yang Z 2016 Bipolar spin-valley diode effect in a silicene magnetic junction *Appl. Phys. Lett.* **109** 122404
[20] Vargiamidis V and Vasilopoulos P 2015 Polarized spin and valley transport across ferromagnetic silicene junctions *J. Appl. Phys.* **117** 094305
[21] Yokoyama T 2013 Controllable valley and spin transport in ferromagnetic silicene junctions *Phys. Rev.* B **87** 241409(R)
[22] Missault N, Vasilopoulos P, Peeters F M and Van Duppen B 2016 Spin- and valley-dependent miniband structure and transport in silicene superlattices *Phys. Rev.* B **93** 125425
[23] Saxena R, Saha A and Rao S 2015 Conductance, valley and spin polarizations, and tunneling magnetoresistance in ferromagnetic–normal–ferromagnetic junctions of silicene *Phys. Rev.* B **92** 245412
[24] Mak K F, He K, Shan J and Heinz T F 2012 Control of valley polarization in monolayer MoS_2 by optical helicity *Nat. Nanotechnol.* **7** 494–8
[25] Liu H *et al* 2015 Observation of intervalley quantum interference in epitaxial monolayer tungsten diselenide *Nat. Commun.* **6** 8180
[26] Lee J, Mak K F and Shan J 2016 Electrical control of the valley Hall effect in bilayer MoS_2 transistors *Nat. Nanotechnol.* **11** 421–5
[27] Zhai X and Jin G 2014 Photoinduced topological phase transition in epitaxial graphene *Phys. Rev.* B **89** 235416
[28] Zhai X and Jin G 2016 Proposal for realizing the quantum spin Hall phase in a gapped graphene bilayer *Phys. Rev.* B **93** 205427
[29] Niu Z-P and Dong S 2014 Valley and spin thermoelectric transport in ferromagnetic silicene junctions *Appl. Phys. Lett.* **104** 202401
[30] Chen X, Zhang L and Guo H 2015 Valley caloritronics and its realization by graphene nanoribbons *Phys. Rev.* B **92** 155427
[31] Zeng M, Feng Y and Liang G 2011 Graphene-based spin caloritronics *Nano Lett.* **11** 1369–73
[32] Gusynin V P, Sharapov S G and Varlamov A A 2014 Anomalous thermospin effect in the low-buckled Dirac materials *Phys. Rev.* B **90** 155107
[33] Chen X, Liu Y, Gu B L, Duan W and Liu F 2014 Giant room-temperature spin caloritronics in spin-semiconducting graphene nanoribbons *Phys. Rev.* B **90** 121403(R)
[34] Inglot M, Dugaev V K and Barnaś J 2015 Thermoelectric and thermospin transport in a ballistic junction of graphene *Phys. Rev.* B **92** 085418
[35] Adachi H, Uchida K-I, Saitoh E and Maekawa S 2013 Theory of the spin Seebeck effect *Rep. Prog. Phys.* **76** 036501
[36] Bauer G E W, Saitoh E and van Wees B J 2012 Spin caloritronics *Nat. Mater.* **11** 391–9
[37] Sinova J, Valenzuela S O, Wunderlich J, Back C H and Jungwirth T 2015 Spin Hall effects *Rev. Mod. Phys.* **87** 1213–59
[38] Hoffmann A and Bader S D 2015 Opportunities at the frontiers of spintronics *Phys. Rev. Applied* **4** 047001
[39] Uchida K, Takahashi S, Harii K, Ieda J, Koshibae W, Ando K, Maekawa S and Saitoh E 2008 Observation of the spin Seebeck effect *Nature* **455** 778–81
[40] Jaworski C M, Yang J, Mack S, Awschalom D D, Heremans J P and Myers R C 2010 Observation of the spin-Seebeck effect in a ferromagnetic semiconductor *Nat. Mater.* **9** 898–903
[41] Uchida K *et al* 2010 Spin Seebeck insulator *Nat. Mater.* **9** 894–7
[42] Wu S M, Zhang W, KC A, Borisov P, Pearson J E, Lederman J S, Hoffmann A and Bhattacharya A 2016 Antiferromagnetic spin Seebeck effect *Phys. Rev. Lett.* **116** 097204
[43] Jaworski C M, Myers R C, Johnston-Halperin E and Heremans J P 2012 Giant spin Seebeck effect in a non-magnetic material *Nature* **487** 210–3
[44] Gorbachev R V *et al* 2014 Detecting topological currents in graphene superlattices *Science* **346** 448–51
[45] Ju L *et al* 2015 Topological valley transport at bilayer graphene domain walls *Nature* **520** 650–5
[46] Shimazaki Y, Yamamoto M, Borzenets I V, Watanabe K, Taniguchi T and Tarucha S 2015 Generation and detection of pure valley current by electrically induced Berry curvature in bilayer graphene *Nat. Phys.* **11** 1032–6
[47] Sui M *et al* 2015 Gate-tunable topological valley transport in bilayer graphene *Nat. Phys.* **11** 1027–31
[48] Gunst T, Markussen T, Stokbro K and Brandbyge M 2016 First-principles method for electron–phonon coupling and electron mobility: applications to two-dimensional materials *Phys. Rev.* B **93** 035414
[49] Wei P *et al* 2016 Strong interfacial exchange field in the graphene/EuS heterostructure *Nat. Mater.* **15** 711–6
[50] Zhai X, Zhang S, Zhao Y, Zhang X and Yang Z 2016 Bipolar spin-valley diode effect in a silicene magnetic junction *Appl. Phys. Lett.* **109** 122404
[51] Zhai X, Gao W, Cai X, Fan D, Yang Z and Meng L 2016 Spin-valley caloritronics in silicene near room temperature *Phys. Rev.* B **94** 245405